Research Article

Maha Abdallah Alnuwaiser, Asmaa M. Elsayed, S. H. Mohamed*, and Mohamed Rabia*

Eco-friendly graphitic carbon nitride–poly(1H pyrrole) nanocomposite: A photocathode for green hydrogen production, paving the way for commercial applications

https://doi.org/10.1515/phys-2024-0104
received September 17, 2024; accepted November 26, 2024

Abstract: The graphitic carbon nitride–poly(1H pyrrole) (g-C_3N_4-P1HP) composite, formed by seeding onto P1HP, is created through a two-step polymerization process of 1H-pyrrole. In the second stage, g-C_3N_4 is incorporated, allowing it to blend within the P1HP matrix. The resulting nanocomposite, composed of nanoscale semi-spherical particles, exhibits remarkable efficiency in capturing photons and facilitating energy transfer between particles, making it an ideal candidate for hydrogen (H_2) gas production. This is particularly effective when using common electrolytes, such as natural seawater from the Red Sea or synthetic seawater produced in the lab. To assess its performance, a three-electrode cell was designed, and the H_2 gas output was measured against current density (J_{ph}). The photocathode achieved a current density of −0.65 mA/cm² in natural seawater and −0.62 mA/cm² in synthetic seawater. The hydrogen generation rates were 16.8 μmol/h in natural seawater and 16.0 μmol/h in synthetic seawater per 10 cm², with the natural electrolyte yielding better results. The photocathode's high sensitivity, efficiency, and environmentally friendly properties – both in materials and electrolytes – underscore the potential of using Red Sea water as a sustainable resource for hydrogen production. These encouraging findings open the door to industrial-scale applications, positioning seawater as a practical solution for renewable hydrogen generation.

Keywords: eco-friendly, poly(1H-pyrrole), hydrogen generation, renewable energy, g-C_3N_4

1 Introduction

Amidst the ongoing Russian–Ukrainian conflict and the resulting energy crisis due to the reduced availability of natural gas and other nonrenewable resources, the world's attention has shifted toward renewable energy sources [1,2]. The limitations of nonrenewable energy, including their harmful environmental by-products, have heightened the need for cleaner alternatives. One of the most promising renewable energy solutions is hydrogen production through water splitting, a process that generates hydrogen gas (H_2), which is considered an excellent fuel source [3–5].

Hydrogen gas, when combusted, produces significant energy without harmful emissions, making it a cleaner alternative to traditional fossil fuels. This energy can be harnessed for a wide range of high-tech applications, including aircraft and spacecraft, due to hydrogen's high energy density. It is also well-suited for everyday uses in factories, homes, and various industries that require a reliable energy source [6–8].

The primary challenge in the large-scale adoption of hydrogen as a fuel lies in the efficient and cost-effective production of H_2 gas. Traditional methods of producing hydrogen are often energy-intensive and costly, limiting its potential for widespread use in economic applications. As a result, researchers and industries are striving to develop more efficient and affordable technologies for water splitting, which would enable the large-scale production of hydrogen while keeping costs down. Water splitting, particularly when driven by renewable energy sources like solar or wind, represents a highly sustainable solution to

* **Corresponding author: S. H. Mohamed**, Physics Department, Faculty of Science, Sohag University, 82524, Sohag, Egypt, e-mail: abo_95@yahoo.com
* **Corresponding author: Mohamed Rabia**, Nanomaterials Science Research Laboratory, Chemistry Department, Faculty of Science, Beni-Suef University, Beni-Suef, 62514, Egypt, e-mail: mohamed chem@science.bsu.edu.eg
Maha Abdallah Alnuwaiser: Department of Chemistry, College of Science, Princess Nourah bint Abdulrahman University, P.O. Box 84428, Riyadh, 11671, Saudi Arabia, e-mail: maalnoussier@pnu.edu.sa
Asmaa M. Elsayed: TH-PPM Group, Physics Department, Faculty of Science, Beni-Suef University, Beni-Suef, 62514, Egypt

the energy crisis. This process involves using electrical energy to break water molecules (H_2O) into their component parts – hydrogen and oxygen. The hydrogen gas can then be stored and used as a clean energy source, while oxygen is released as a by-product. By relying on nature's power to drive this reaction, hydrogen production through water splitting has the potential to significantly reduce greenhouse gas emissions and reliance on fossil fuels [1,9].

However, the key to unlocking hydrogen's full potential lies in overcoming the technical and economic barriers associated with its production. Advances in photocatalytic materials, electrocatalysts, and membrane technology are critical to improving the efficiency of water splitting. Researchers are exploring various materials and techniques, including the use of new photocathodes, nanostructures, and hybrid materials, to enhance the conversion of solar energy into hydrogen [10,11]. These innovations could drive down costs and make hydrogen a more viable option for large-scale energy applications. In addition to technological advancements, scaling up hydrogen production will require significant infrastructure investments. Storage, transportation, and distribution networks need to be developed to accommodate hydrogen as a mainstream energy source. Governments and industries will need to collaborate to establish the necessary infrastructure while ensuring the transition to hydrogen remains economically feasible.

To achieve high efficiency, materials with large surface areas, such as carbon derivatives, are essential. One such material, graphitic carbon nitride (g-C_3N_4), is highly regarded for its sheet-like morphology, which makes it an excellent candidate for composite formation with other materials. g-C_3N_4 possesses valuable optical and electrical properties, largely due to the movement of hot electrons across its surface. This material is frequently used as an alternative to oxides or sulfides because carbon-based materials typically offer a better volume-to-mass ratio, which enhances their performance in certain applications [5,12].

The unique properties of g-C_3N_4 are especially notable in the realm of conjugated polymers. The electron localization on its surface contributes to its versatility, making it ideal for both optical and electrical applications. As a result, g-C_3N_4 has gained significant attention for its potential in advanced technologies [13,14]. Polypyrrole (Ppy), for example, is a promising conjugated polymer known for its small particle size and diverse morphologies, which enhance its applicability in various techniques and industries. In a study conducted by Atta *et al.*, a composite was created using P1HP with graphene oxide (GO) or nickel oxide (NiO). The results demonstrated impressive photovoltaic properties, with the estimated photocurrent density (J_{ph}) values reaching 0.1 and 0.2 mA/cm^2 under light conditions [15,16]. The P1HP polymer played a crucial dual role as both a coating material and a semiconductor, further highlighting the potential of such polymers in enhancing the efficiency of various applications, particularly in the fields of energy conversion and electronic devices. The major drawback related to other studies relies on external electrolytes rich in protons, such as highly acidic or basic solutions, or neutral electrolytes like Na_2SO_4 [8,17–20].

In this study, an eco-friendly C_3N_4-P1HP nanocomposite, integrated with P1HP, has been developed as an efficient photocathode for hydrogen (H_2) gas production *via* electrolysis. By utilizing an unconventional electrolyte – natural seawater – this sustainable and cost-effective method holds significant potential for H_2 generation. The photocathode's properties were thoroughly analyzed, with electrical performance assessed through linear sweep voltammetry and chronoamperometry (time-current) measurements, tested in both natural and artificial seawater. Additionally, the photocurrent density (J_{ph}) was evaluated under different photon energies, and key efficiency parameters such as the incident photon-to-current efficiency (IPCE) and H_2 production rates were calculated. The photocathode's remarkable sensitivity, high efficiency, and eco-friendly nature, in terms of both materials and electrolytes, highlight its potential for large-scale hydrogen production. These promising findings suggest that Red Sea water could serve as a sustainable resource for H_2 generation, paving the way for industrial applications and advancing renewable energy development.

2 Materials and methods

2.1 Materials

Pyrrole (Across Co., 99.9%, USA), urea (99.9%, Pio-Chem co, Egypt), HCl (36%, Merck, Germany), ethanol (C_2H_5OH, 99.9%, Merck, Germany), and $(NH_4)_2S_2O_8$ (99.9%, Pio-Chem co, Egypt) were used in this study.

2.2 Fabrication of the P1HP-g-C_3N_4/P1HP photocathode

The fabrication of the P1HP-g-C_3N_4/P1HP photocathode begins with the deposition of the P1HP-g-C_3N_4 layer on a P1HP film, which serves as a promising seeding layer. The detailed analysis and characterization of this seeding layer are based on our previous studies [21,22]. This layer is essential for the subsequent deposition process, in which the P1HP-g-C_3N_4

film is formed through the oxidation of pyrrole with insite g-C_3N_4 nanosheets. g-C_3N_4 is prepared by combusting 5.0 g of urea in a nitrogen atmosphere at 550°C for 2 h. After combustion, g-C_3N_4 is ground into a fine powder. A portion of this material, specifically 0.05 g, is then suspended in 50 ml of water along with 0.06 mol of 1H-pyrrole.

Meanwhile, an oxidizing agent, $(NH_4)_2S_2O_8$, at a concentration of 0.15 M, is stirred until it forms a clear solution. This oxidant is added to the monomer containing the suspended g-C_3N_4 and pyrrole. This oxidant initiates the polymerization reaction, resulting in the formation of the P1HP-g-C_3N_4 film on the P1HP substrate. The final product is the P1HP-g-C_3N_4/P1HP photocathode, which undergoes further treatment to prepare it for analysis (Figure 1(a) and (b)). Once prepared, this photocathode is ready to be integrated into a three-electrode cell for application testing. The combination of P1HP and g-C_3N_4 in this structure is anticipated to enhance the photocathode's performance as a candidate for further study and potential use in photoelectrochemical systems.

2.3 Synthesis of photoelectrochemically green hydrogen using the P1HP-g-C_3N_4/P1HP photocathode

Using Red Sea water as an electrolyte offers numerous advantages due to the unique behavior of this natural water, particularly its content of heavy metals. These heavy metals enhance the electrolyte's performance, facilitating extensive ion movement, which in turn significantly activates hydrogen gas generation. To specifically examine the impact of these heavy metals on H_2 production without introducing any additional by-products or side reactions, artificial seawater free of heavy metals is used for comparison. This artificial seawater is formulated with a precise chemical composition of $KHCO_3$ (0.24 g/l), $CaCl_2$ (2.43 g/l), NaCl (38.38 g/l), $MgCl_2$ (19.06 g/l), and Na_2SO_4 (5.26 g/l) [23].

The fabricated P1HP-g-C_3N_4/P1HP photocathode is then employed within a three-electrode cell to drive the main reduction reaction responsible for H_2 gas generation

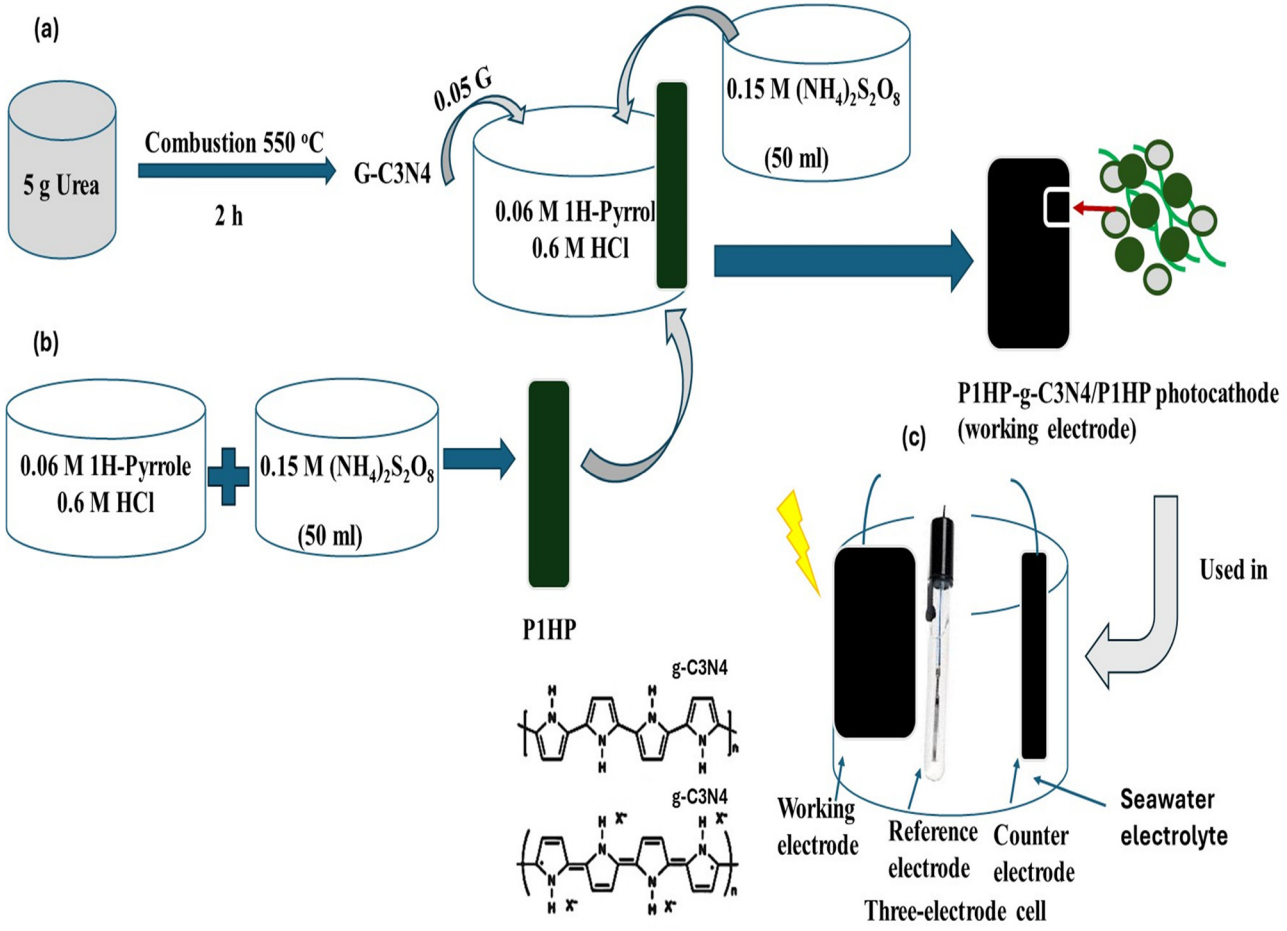

Figure 1: (a) and (b) The fabrication and (c) photoelectrochemical testing of the g-C_3N_4-P1HP/P1HP photocathode using the three-electrode cell for H_2 gas generation.

through water splitting (Figure 1(c)). The initial step in this reduction process involves the formation of hydroxyl ($OH^{\cdot}$) radicals. The cell also contains two additional electrodes: a counter graphite electrode, which serves as an inert conductor to facilitate electrical conductivity, and a reference calomel electrode, which provides a stable potential to the cell.

Illumination for the reaction is supplied by a white light vacuum metal halide lamp chosen for its ability to emit a broad spectrum of photons. To achieve precise control over the photon energies and frequencies, optical filters are used. The efficiency and sensitivity of the fabricated photocathode are assessed by measuring the photocurrent density (J_{ph}) under both monochromatic light and full-spectrum white light. These measurements are conducted using linear sweep voltammetry, and the relationship between chopped current and time is also evaluated to provide further insight into the photocathode's performance. The amount of H_2 generated is quantified using Eq. (1) [17]. On the other hand, the IPCE is estimated using Eq. (2) based on the current density relative to the source light intensity (P) and wavelength (λ). Overall, this experimental setup demonstrates an effective method for producing hydrogen gas through the splitting of Red Sea water, highlighting the potential of this approach for sustainable H_2 generation. The presence of heavy metals in Red Sea water plays a crucial role in enhancing the efficiency of the electrolyte, thereby improving the overall hydrogen production process:

$$H_2\text{mole} = \int_0^t J_{ph} \cdot dt/F, \tag{1}$$

$$\text{IPCE} = 1{,}240 J_{ph}/P \cdot \lambda. \tag{2}$$

3 Results and discussion

3.1 Physicochemical analysis of the P1HP-g-C_3N_4 nanocomposite

The surface features and overall topography of the fabricated P1HP-g-C_3N_4 nanocomposite, in comparison to the g-C_3N_4 material alone, are illustrated in Figure 2. The SEM image in Figure 2(a) reveals the semi-spherical nanoscale particles of approximately 150 nm in size. These particles of P1HP are uniformly coated on the g-C_3N_4 sheets, resulting in a structure with significant porosity. This porous nature of the P1HP-g-C_3N_4 nanocomposite makes it highly effective at trapping photons, as the spherical particles facilitate multiple photon interactions, thereby enhancing photon absorption.

The TEM image shown in Figure 2(b) is used to further assess the coating and compactness of P1HP on the g-C_3N_4 sheets. This image clearly shows the g-C_3N_4 sheets acting as the core material while the P1HP forms a shell around them. This core–shell configuration is evident from the variation in the color of the materials in the TEM image, highlighting the strong compacting process between P1HP and the g-C_3N_4 sheets.

For a deeper understanding of this behavior, theoretical modeling is used to simulate the compacting process (Figure 2(c)). The model reveals that the P1HP particles appear as bright spots distributed over the g-C_3N_4 sheets, which are depicted as darker regions. The total diameter of these combined structures is around 300 nm, with the g-C_3N_4 sheets themselves being about 250 nm in diameter and less than 20 nm in length. This theoretical model aligns well with the observed experimental data.

The morphology of the g-C_3N_4 sheets is further characterized, showing them as thin sheets with the aforementioned dimensions (Figure 2(d)). The successful integration of these distinct morphologies into the P1HP-g-C_3N_4 nanocomposite underscores its potential as a promising material. The combination of the P1HP's spherical particles and the g-C_3N_4 sheets results in a nanocomposite with enhanced structural and functional properties, making it a valuable candidate for applications requiring efficient photon absorption and other related functions.

The FTIR spectroscopy analysis of the synthesized P1HP-g-C_3N_4 nanocomposite, relative to the pure P1HP material, is presented in Figure 3(a). The specific functional groups within this nanocomposite, following the incorporation of g-C_3N_4, are detailed in this figure. The observed changes in the band positions and intensities upon the introduction of g-C_3N_4 indicate a strong chemical interaction between P1HP and g-C_3N_4 during the polymerization process. This interaction is particularly evident through the emergence of new bands, such as the one at 661 cm^{-1}, and the significant intensities observed at 880 and 1,401 cm^{-1}.

Moreover, the main functional groups characteristic of P1HP are still present, including those associated with the ring structures at 880, 1,059, 1,181, 1,288, 1,401, 1,639, and 1,713 cm^{-1}. These functional groups appear at similar positions in the pristine P1HP polymer, indicating that the polymer structure has been successfully maintained even after the incorporation of g-C_3N_4. The detailed list and summary of these observed functional groups are provided in Table 1. The variations in the FTIR spectra, specifically the shifts in band positions and changes in intensities, provide strong evidence of the successful integration of g-C_3N_4 into the P1HP matrix. This integration is accompanied by the formation of new chemical bonds,

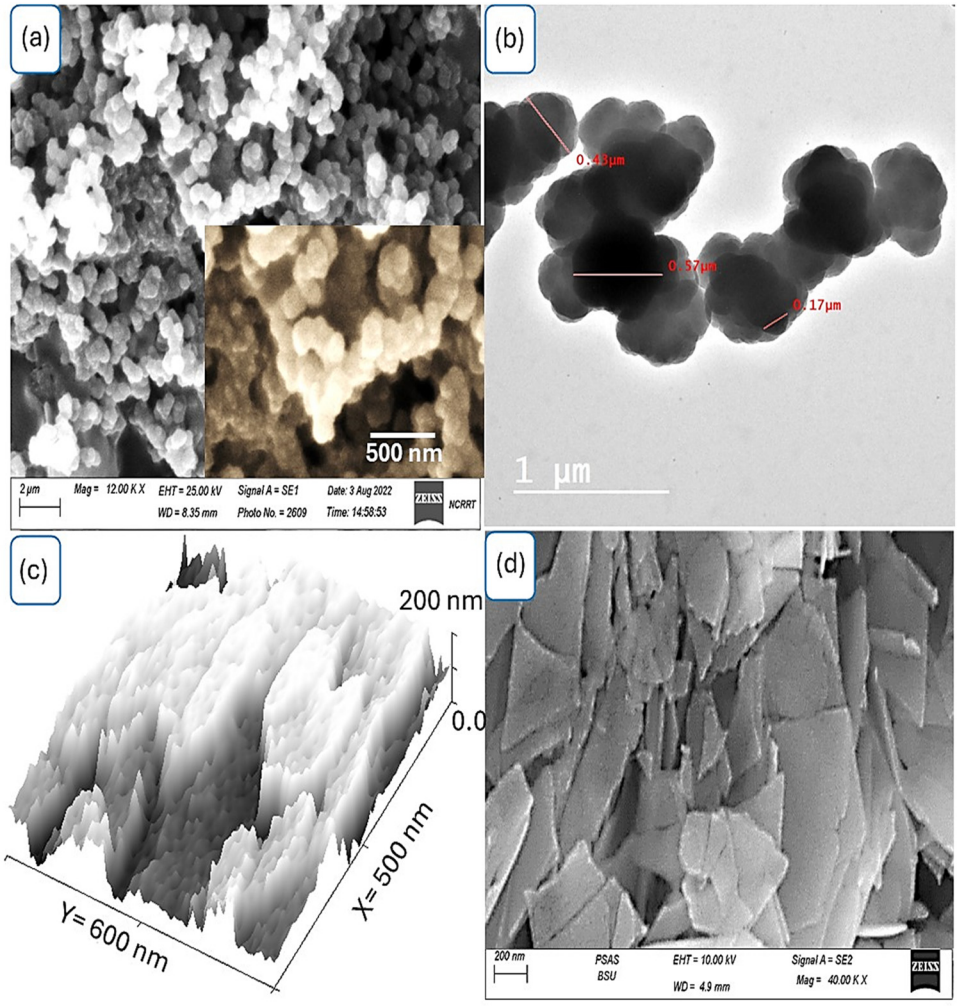

Figure 2: Topography and morphological analyses of the fabricated P1HP-g-C_3N_4 nanocomposite: (a) SEM, (b) TEM, (c) theoretical roughness, and (d) SEM of g-C_3N_4.

suggesting a well-established interaction between the two components, which is crucial for the enhanced properties of the nanocomposite.

The XRD analysis of the P1HP-g-C_3N_4 nanocomposite estimates the distinct components of the composite, where g-C_3N_4 serves as the primary crystalline material. As depicted in Figure 3(b), g-C_3N_4 exhibits two prominent peaks at 13.0° and 27.2° for the (100) and (002) crystal planes, respectively. These peaks reflect the crystalline behavior and growth orientation of the g-C_3N_4 within the composite. In contrast, the pristine P1HP polymer shows a broad peak at 26.6°, signifying its amorphous structure. This broad peak reflects the lack of crystallinity in the P1HP polymer, highlighting its amorphous characteristics. However, after the formation of the nanocomposite, the peaks for g-C_3N_4 remain, indicating that the crystalline g-C_3N_4 is chemically connected inside the composite. Additionally, the XRD analysis reveals the emergence of a new broad peak at 32.7°, which points to the crystallinity enhancement of the polymer network after chemical connections with g-C_3N_4. Therefore, g-C_3N_4 not only maintains its crystalline nature but also improves the overall structural order of the nanocomposite.

XPS analysis, presented in Figure 3(c), serves to illustrate the key elements anticipated in the composite material. Through this analysis, the primary components of the pristine P1HP polymer are identified, particularly carbon (C) and nitrogen (N), which are clearly visible at binding energies of 284.8 and 400 eV, respectively. These peaks correspond to the 1s orbitals of carbon and nitrogen, signifying their presence and integration within the polymer matrix. Further, Figure 3(d) focuses on the identification of carbon by estimating the positions of C–C and C═C bonds, which are characteristic of the pristine polymer structure. These observations further validate the contribution of

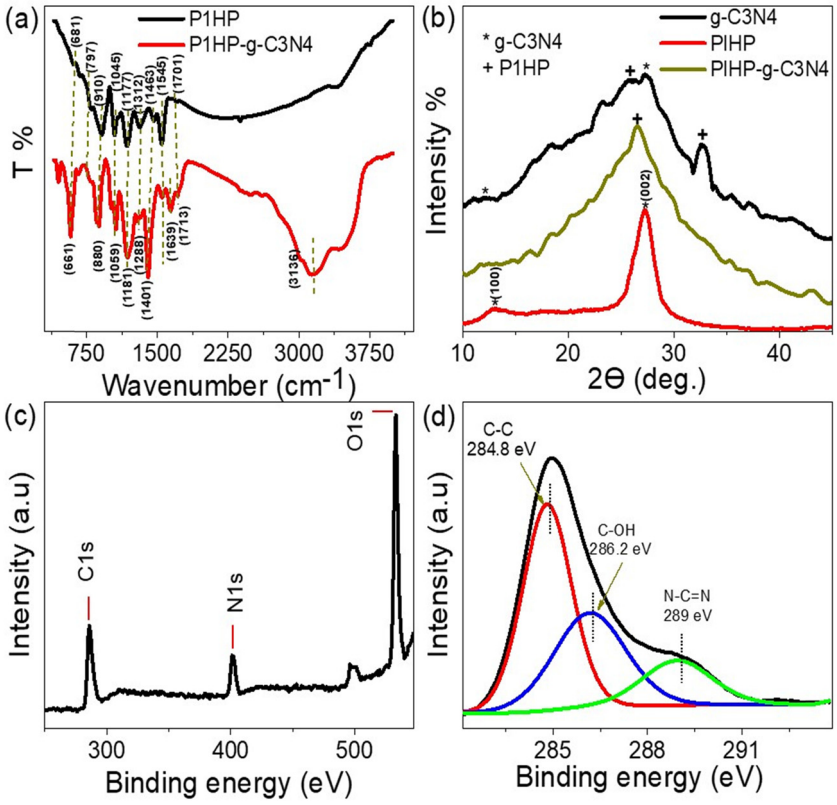

Figure 3: Chemical analysis of the P1HP-g-C_3N_4 nanocomposite: (a) FTIR. (b) XRD, and (c) and (d) XPS analyses, which provide a comprehensive survey and focus on the C element.

Table 1: Summary of the observed groups from FTIR data using the chart

Group and its value (cm^{-1})		Functional group
P1HP-g-C_3N_4	**P1HP**	
661, 880, 1,401	—	g-C_3N_4
880	910	C–H out of plane
1,059, 1,181	1,045, 1,177	C–H
1,288	1,312	C–N
1,401	1,463	C–C
1,639, 1,713	1,545, 1,701	C═C

carbon in maintaining the structural integrity of the P1HP polymer.

In addition to carbon and nitrogen, oxygen (O) emerges as a crucial element within the composite, primarily associated with g-C_3N_4, as seen at a binding energy of 532.1 eV. Oxygen plays a critical role in enhancing the material's functionality, particularly in interactions involving the g-C_3N_4 structure. Furthermore, the analysis identifies other important groups within the composite. The C–OH group is observed at a binding energy of 286.2 eV, while the N–C═N group is detected at 289 eV [24], both of which are estimated, as shown in Figure 3(d). These groups contribute to the overall chemical stability and performance of the nanocomposite. The XPS data provide a detailed understanding of the elemental composition and the functional groups present in the material. This information is essential for confirming the distribution and significance of the elements within the composite, particularly their roles in contributing to the structural and functional properties of the P1HP material. As such, the analysis underscores the importance of these elements in enhancing the material's overall characteristics, making it suitable for various applications.

3.2 P1HP-g-C_3N_4/P1HP photocathode for electrochemical estimation

The fabricated P1HP-g-C_3N_4/P1HP photocathode was tested in a photoelectrochemical setup using a three-electrode cell to remove H_2 gas from either natural or artificial seawater as an electrolyte. Natural seawater, in particular, is a cost-effective and abundant option, making it an attractive

choice for industrial applications. Its chemical composition, which includes heavy metals, plays a critical role in the electrolysis process, serving as a sacrificial agent. The mobility of these heavy metals enhances electrolysis, driving the H_2 gas production reaction.

To better understand the specific contribution of natural seawater, a comparative study was conducted using artificial seawater that is free of heavy metals. This experiment aimed to clarify whether the presence of heavy metals in natural seawater exclusively promotes hydrogen generation without triggering additional reactions like metal deposition or redirecting the applied voltage to other unintended processes. By comparing the outcomes of these two electrolytes, the distinct role of natural seawater in motivating hydrogen production was assessed.

The structural and functional properties of the fabricated photocathode, composed of semiconductor materials, were also thoroughly evaluated. The g-C_3N_4 materials were embedded within the P1HP polymer network, with the P1HP structure offering strong anti-corrosion properties. This integration provided the semiconductor properties required for effective photoelectrochemical reactions. Electron clouds accumulated over the P1HP polymer, which enhanced the interaction between the photocathode and seawater and initiated the hydrogen generation process. During the reaction, hydroxyl radicals (OH^-) formed within the water, and through a series of sequential mechanisms, hydrogen gas was produced. The resulting current was measured, with J_{ph} indicating the rate of hydrogen gas generation.

The key driver of these reactions is the generation of hot electrons on the surface of the photocathode, which facilitates the hydrogen evolution reaction [25,26]. Meanwhile, the corresponding holes migrated in the opposite direction toward the counter electrode. This flow of charge carriers allowed the photocathode to operate efficiently in the electrolysis process, harnessing seawater's chemical properties to produce H_2 gas. Through this experimental setup, the full potential of the P1HP-g-C_3N_4/P1HP photocathode for hydrogen production from seawater was realized, offering insights into its suitability for large-scale, economically viable hydrogen generation. To evaluate the behavior of the P1HP-g-C_3N_4/P1HP photocathode when using natural or artificially prepared seawater as an electrolyte, electrochemical measurements were performed both under dark conditions and light illumination, as shown in Figure 4(a). The current density values obtained were −0.62 mA/cm² for artificial seawater and −0.65 mA/cm² for natural seawater. The slight improvement in performance with natural seawater highlights its potential as a sustainable resource for renewable energy generation and future industrial applications. This enhanced performance is likely due to the natural heavy metals in seawater, which act as self-sacrificing agents. These agents eliminate the need for additional external electrolytes, making natural seawater a more efficient and environmentally friendly choice for this process.

The high sensitivity of the P1HP-g-C_3N_4/P1HP photocathode is further demonstrated by its ability to sense and respond to any changes in light exposure. When subjected to alternating cycles of light (on) and dark (off) conditions, there is a significant change in the produced current density, indicating the photocathode's capability to absorb photons effectively (Figure 4(b)). This process leads to the generation of electron–hole pairs, motivating the splitting reaction [27]. The reversible movement of these electrons and holes under light exposure further confirms the photocathode's efficiency in capturing and utilizing light energy. This sequential change in the current density during chopped light experiments reflects the material's robust performance in photoelectrochemical reactions for the energy generation through seawater.

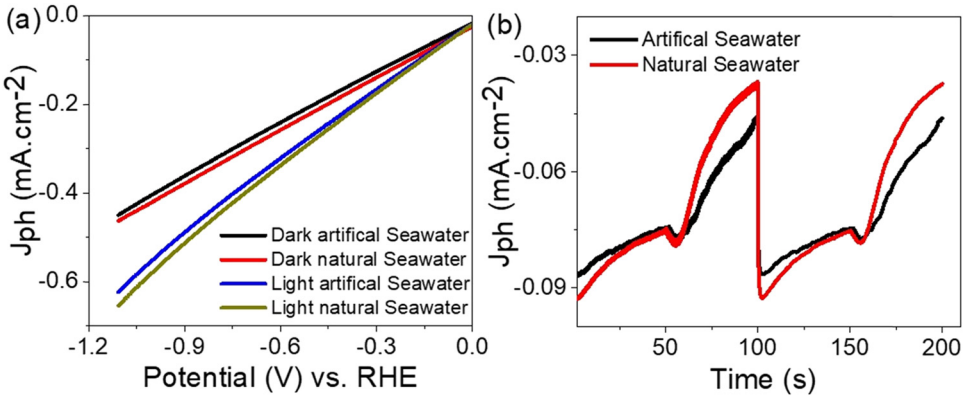

Figure 4: (a) Electrochemical assessment and (b) chopped on/off light illumination test for the fabricated P1HP-g-C_3N_4/P1HP photocathode using natural or artificial seawater at room temperature.

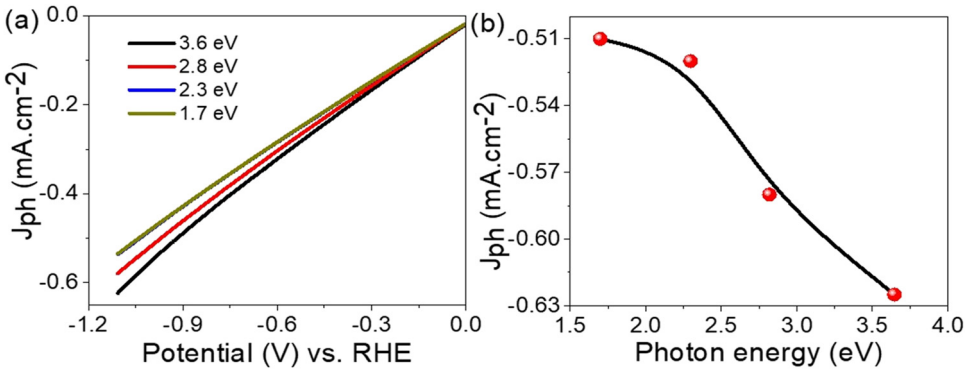

Figure 5: (a) Electrochemical assessment and (b) estimated values at −1.1 V for the fabricated P1HP-g-C_3N_4/P1HP photocathode using natural seawater using various photon energies at room temperature.

The behavior of the P1HP-g-C_3N_4/P1HP photocathode demonstrates its ability to efficiently participate in energy conversion processes, particularly in splitting water for hydrogen generation. The use of natural seawater as an electrolyte enhances this efficiency, as the natural heavy metals present act as sacrificial agents. This reduces the need for adding external electrolytes, making the process more cost-effective and sustainable. Additionally, the photocathode shows excellent sensitivity to light, as evidenced by its rapid and significant response to changes in light intensity. The repeated on-and-off cycles of light exposure result in considerable variations in current density, underscoring the material's high photon absorption capacity.

Given the superior performance of natural seawater H_2 gas generation compared to artificially prepared water, the effectiveness of this natural water was further tested under different photon energy levels. Photon energy serves as the primary driver for the water-splitting reaction, transferring energy to the P1HP-g-C_3N_4/P1HP photocathode. This energy is then utilized in the splitting process. As the photon energy varies, the amount of H_2 gas produced changes accordingly. With an increase in photon energy, the photocathode's surface accumulates more hot electrons, which play a crucial role in driving the reaction. The residual energy from the photon transfer is converted into kinetic energy [21,28], which accelerates the electrons and enhances the production of H_2 gas. Figure 5(a) illustrates this behavior, where the produced current density (J_{ph}) increases in direct correlation with an increase in photon energy. This trend is summarized in Figure 5(b), which shows that the optimal performance is observed at a photon energy of 3.6 eV, yielding a current density of −0.63 mA/cm^2. As the photon energy decreases to 440 nm, the current density drops slightly to −0.58 mA/cm^2. The lowest current densities are recorded at photon energies corresponding to wavelengths of 540 and 730 nm. These findings highlight the importance of using higher energy photons in the process, as they enhance H_2 gas production by interacting more effectively with the splitting levels of the P1HP-g-C_3N_4/P1HP photocathode. Higher photon energies result in greater electron excitation and a more efficient water-splitting reaction, leading to increased hydrogen

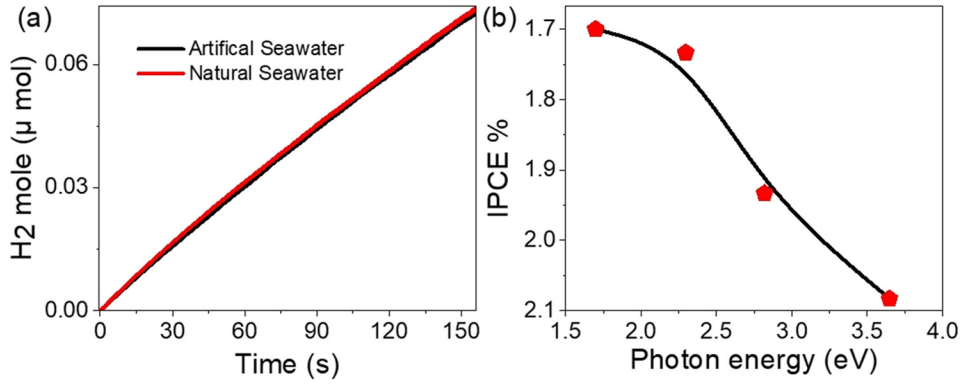

Figure 6: (a) Moles of H_2 gas produced using artificial and natural seawater, and (b) IPCE measured in natural seawater for the P1HP-g-C_3N_4/P1HP photocathode.

Table 2: P1HP-g-C_3N_4/P1HP photocathode performance of H_2 gas relative to other studies

Photoelectrode	Electrolyte	J_{ph} (mA/cm^2)
Mn(IV) oxide/Mn (IV) sulfide/poly-2-amino-1-mercaptobenzene [29]	Sewage water	0.33
Ppy/GO [16]	Sewage water	0.1
Ppy/NiO [15]	Sewage water	0.11
Cr_2S_3-Cr_2O_3/Poly-2-aminobenzene-1-thiol [30]	Sewage water	0.017
Poly-3-methyl aniline/GO [31]	Sewage water	0.09
Poly-O-aminothiophenol/iodide [32]	Red Sea water	0.12
P1HP-g-C_3N_4/P1HP (this work)	Natural seawater	0.65
	Artificial seawater	0.62

generation. Consequently, it is recommended to optimize the hydrogen generation process by utilizing photons with higher energy levels, as this maximizes the efficiency of the photocathode under such conditions.

The H_2 mole efficiency parameters for the P1HP-g-C_3N_4/P1HP photocathode are evaluated using Eq. (1) and Figure 6(a), while the IPCE is determined based on Eq. (2) and Figure 6(b). The key factor in this estimation is the current density, which indicates the moles of H_2 gas produced. Figure 6(a) reveals that this photocathode demonstrates superior performance in natural seawater compared to artificial seawater prepared in the lab, with estimated moles of 16.8 and 16.0 μmol/h per 10 cm^2, respectively. This highlights the enhanced electrolyte properties of natural seawater, where heavy metals contribute to better ion mobility, leading to more efficient electrolysis.

The IPCE of the photocathode in natural seawater is shown in Figure 6(b), achieving 2.09% efficiency under 3.6 eV photon illumination. The efficiency decreases to 1.94% at 2.8 eV and further to 1.74% at 2.3 eV. This trend illustrates the photocathode's high sensitivity to varying photon energy, with a noticeable change in IPCE as the photon energy shifts.

Given these impressive results, a comparison with previous studies is presented in Table 2, demonstrating the photocathode's superior performance. This eco-friendly study utilizes both sustainable materials and natural seawater as the electrolyte, underscoring the potential for large-scale industrial applications. The photocathode's high efficiency suggests that seawater can be a viable renewable energy source, opening new possibilities for its use in energy production.

4 Conclusions

The g-C_3N_4-P1HP nanocomposite, integrated with P1HP, is designed as an efficient photocathode for H_2 gas production through electrolysis. Using an unconventional electrolyte – natural seawater – this eco-friendly and cost-effective approach shows great promise for H_2 generation. The nanocomposite is composed of nanoscale semi-spherical particles, which are highly effective at trapping photons and facilitating energy transfer between composite particles. This makes g-C_3N_4-P1HP an ideal material for H_2 gas production, particularly when utilizing readily available electrolytes like natural seawater from the Red Sea or lab-prepared artificial seawater.

In performance tests, the photocathode achieved a J_{ph} of −0.65 mA/cm^2 in natural seawater and −0.62 mA/cm^2 in artificial seawater. The corresponding H_2 production rates were 16.8 μmol/h for natural seawater and 16.0 μmol/h for artificial seawater per 10 cm^2, demonstrating the superior efficiency of the natural electrolyte. The photocathode also exhibits high sensitivity, responding differently to various photon energies, highlighting its ability to maintain efficient performance under varying conditions.

The combination of this photocathode's sensitivity, efficiency, and eco-friendly attributes in both materials and electrolytes underscores its potential for large-scale hydrogen production. These promising results point to the possibility of using Red Sea water as a sustainable resource for H_2 gas generation, opening the door to industrial applications and contributing to the development of renewable energy sources.

Acknowledgments: Princess Nourah bint Abdulrahman University Researchers Supporting Project number (PNURSP2024R186), Princess Nourah bint Abdulrahman University, Riyadh, Saudi Arabia.

Funding information: Princess Nourah bint Abdulrahman University Researchers Supporting Project number (PNURSP2024R186), Princess Nourah bint Abdulrahman University, Riyadh, Saudi Arabia.

Author contributions: Mohamed Rabia: experimental and writing; Maha Abdallah Alnuwaiser: writing, funding, and

supervision; and Asmaa M. Elsayed and SH Mohamed: supervision and ordering the work. All authors have accepted responsibility for the entire content of this manuscript and approved its submission.

Conflict of interest: The authors state no conflict of interest.

Data availability statement: All data generated or analyzed during this study are included in this published article.

References

[1] Oshiro K, Fujimori S. Limited impact of hydrogen co-firing on prolonging fossil-based power generation under low emissions scenarios. Nat Commun. 2024;15(1):1–11. doi: 10.1038/s41467-024-46101-5.

[2] Potashnikov V, Golub A, Brody M, Lugovoy O. Decarbonizing Russia: Leapfrogging from fossil fuel to hydrogen. Energies. 2022;15:683. doi: 10.3390/EN15030683.

[3] El ouardi M, Idrissi AE, Ahsaine HA, BaQais A, Saadi M, Arab M. Current advances on nanostructured oxide photoelectrocatalysts for water splitting: A comprehensive review. Surf Interfaces. 2024;45:103850. doi: 10.1016/J.SURFIN.2024.103850.

[4] Sharifi T, Ghayeb Y, Mohammadi T, Momeni MM. Enhanced photoelectrochemical water splitting of CrTiO2 nanotube photoanodes by the decoration of their surface via the photodeposition of Ag and Au. Dalton Trans. 2018;47:11593–604. doi: 10.1039/C8DT02383B.

[5] Mishra A, Basu S, Shetti NP, Reddy KR, Aminabhavi TM. Photocatalysis of graphene and carbon nitride-based functional carbon quantum dots. In Nanoscale materials in water purification; 2019. p. 759–81. doi: 10.1016/B978-0-12-813926-4.00035-5.

[6] Jovičević-Klug M, Souza Filho IR, Springer H, Adam C, Raabe D. Green steel from red mud through climate-neutral hydrogen plasma reduction. Nature. 2024;625(7996):703–9. doi: 10.1038/s41586-023-06901-z.

[7] Giuntoli F, Menegon L, Siron G, Cognigni F, Leroux H, Compagnoni R, et al. Methane-hydrogen-rich fluid migration may trigger seismic failure in subduction zones at forearc depths. Nat Commun. 2024;15(1):1–16. doi: 10.1038/s41467-023-44641-w.

[8] Giovanniello MA, Cybulsky AN, Schittekatte T, Mallapragada DS. The influence of additionality and time-matching requirements on the emissions from grid-connected hydrogen production. Nat Energy. 2024;2024:1–11. doi: 10.1038/s41560-023-01435-0.

[9] Mallikarjuna K, Rafiqul Bari GAKM, Vattikuti SVP, Kim H. Synthesis of carbon-doped SnO2 nanostructures for visible-light-driven photocatalytic hydrogen production from water splitting. Int J Hydrog Energy. 2020;45:32789–96. doi: IJHYDENE.2020.02.176">10.1016/J.IJHYDENE.2020.02.176.

[10] Morales-Guio CG, Tilley SD, Vrubel H, Graẗzel M, Hu X. Hydrogen evolution from a copper(I) oxide photocathode coated with an amorphous molybdenum sulphide catalyst. Nat Commun. 2014;5(1):1–7. doi: 10.1038/ncomms4059.

[11] Wu S, Sun J, Li Q, Hood ZD, Yang S, Su T, et al. Effects of surface terminations of 2D Bi2WO6 on photocatalytic hydrogen evolution from water splitting. ACS Appl Mater Interfaces. 2020;12:20067–4. doi: 10.1021/ACSAMI.0C01802/SUPPL_FILE/AM0C01802_SI_001.PDF.

[12] Afshari M, Dinari M, Momeni MM. The graphitic carbon nitride/polyaniline/silver nanocomposites as a potential electrocatalyst for hydrazine detection. J Electroanal Chem. 2019;833:9–16. doi: 10.1016/J.JELECHEM.2018.11.022.

[13] Haryński Ł, Olejnik A, Grochowska K, Siuzdak K. A facile method for Tauc exponent and corresponding electronic transitions determination in semiconductors directly from UV–Vis spectroscopy data. Opt Mater. 2022;127:112205. doi: 10.1016/J.OPTMAT.2022.112205.

[14] Lee JH, Lee WW, Yang DW, Chang WJ, Kwon SS, Park WIL. Anomalous photovoltaic response of graphene-on-GaN Schottky photodiodes. ACS Appl Mater Interfaces. 2018;10:14170–74. doi: 10.1021/acsami.8b02043.

[15] Atta A, Negm H, Abdeltwab E, Rabia M, Abdelhamied MM. Facile fabrication of polypyrrole/NiOx core-shell nanocomposites for hydrogen production from wastewater. Polym Adv Technol. 2023;34:1633. doi: 10.1002/PAT.5997.

[16] Hamid MMA, Alruqi M, Elsayed AM, Atta MM, Hanafi HA, Rabia M. Testing the photo-electrocatalytic hydrogen production of polypyrrole quantum dot by combining with graphene oxide sheets on glass slide. J Mater Sci: Mater Electron. 2023;34:1–11. doi: 10.1007/S10854-023-10229-9/METRICS.

[17] Rabia M, Aldosari E, Geneidy AHA. Exceptionally crystalline nature of CrO3-Cr2O3/Ppy nanocomposite as a prospective photoelectrode for efficient green hydrogen generation in the context of environmentally friendly water-splitting reactions using sanitized water. Environ Prog Sustain Energy. 2024;43:e14455. doi: 10.1002/EP.14455.

[18] Tsao CW, Narra S, Kao JC, Lin YC, Chen CY, Chin YC, et al. Dual-plasmonic Au@Cu7S4 Yolk@shell nanocrystals for photocatalytic hydrogen production across visible to near infrared spectral region. Nat Commun. 2024;15(1):1–13. doi: 10.1038/s41467-023-44664-3.

[19] Constantinou P, Stock TJZ, Tseng L-T, Kazazis D, Muntwiler M, Vaz CAF, et al. EUV-induced hydrogen desorption as a step towards large-scale silicon quantum device patterning. Nat Commun. 2024;15(1):1–13. doi: 10.1038/s41467-024-44790-6.

[20] Kountouris I, Bramstoft R, Madsen T, Gea-Bermúdez J, Münster M, Keles D. A unified european hydrogen infrastructure planning to support the rapid scale-up of hydrogen production. Nat Commun. 2024;15(1):1–13. doi: 10.1038/s41467-024-49867-w.

[21] Aldosari E, Rabia M, Abdelazeez AAA. Rod-shaped Mo (VI) trichalcogenide – Mo (VI) oxide decorated on poly (1-H pyrrole) as a promising nanocomposite photoelectrode for green hydrogen generation from sewage water with high efficiency. Green Process Synth. 2024;13:20230243.

[22] Rabia M, Elsayed AM, Alnuwaiser MA. Highly morphological behavior AgI/P1HP intercalated with iodide ions in the polymer chains as a promising photocathode for the hydrogen generation from Red Sea Water. Opt Quantum Electron. 2024;56:1–16. doi: 10.1007/S11082-023-06274-7/METRICS.

[23] Moradi-Alavian S, Kazempour A, Mirzaei-Saatlo M, Ashassi-Sorkhabi H, Mehrdad A, Asghari E, et al. Promotion of hydrogen evolution from seawater via poly(aniline-Co-4-nitroaniline) combined with 3D nickel nanoparticles. Sci Rep. 2023;13:1–10. doi: 10.1038/s41598-023-48355-3.

[24] Gong S, Jiang Z, Zhu S, Fan J, Xu Q, Min Y. The synthesis of graphene-TiO2/g-C3N4 super-thin heterojunctions with enhanced

visible-light photocatalytic activities. J Nanopart Res. 2018;20:1–13. doi: 10.1007/S11051-018-4399-8/FIGURES/7.

[25] Zhao C, Yu Z, Xing J, Zou Y, Liu H, Zhang H, et al. Effect of Ag2s nanocrystals/reduced graphene oxide interface on hydrogen evolution reaction. Catalysts. 2020;10:1–12. doi: 10.3390/catal10090948.

[26] Du L, Shi G, Zhao Y, Chen X, Sun H, Liu F, et al. Plasmon-promoted electrocatalytic water splitting on metal-semiconductor nanocomposites: The interfacial charge transfer and the real catalytic sites. Chem Sci. 2019;10:9605–12. doi: 10.1039/c9sc03360b.

[27] Kanwal F, Rani I, Batool A, Sandali Y, Li C, Shafique S, et al. Enhanced dielectric and photocatalytic properties of TiO2-decorated RGO/PANI hybrid composites synthesized by in-situ chemical oxidation polymerization route. Mater Sci Eng: B. 2023;298:116837. doi: 10.1016/J.MSEB.2023.116837.

[28] Xia Z, Tao Y, Pan Z, Shen X. Enhanced photocatalytic performance and stability of 1T MoS2 transformed from 2H MoS2 via Li Intercalation. Results Phys. 2019;12:2218–24. doi: 10.1016/J.RINP.2019.01.020.

[29] Rabia M, Elsayed AM, Alnuwaiser MA. Mn (IV) oxide/Mn (IV) sulfide/poly-2-amino-1-mercaptobenzene for green hydrogen generation. Surf Innov. 2023;12(5–6):282–91. doi: 10.1680/JSUIN.23.00031.

[30] Rabia M, Elsayed AM, Alnuwaiser MA. Cr2S3-Cr2O3/poly-2-aminobenzene-1-thiol as a highly photocatalytic material for green hydrogen generation from sewage water. Micromachines. 2023;14:1567. doi: 10.3390/MI14081567.

[31] Helmy A, Rabia M, Shaban M, Ashraf AM, Ahmed S, Ahmed AM. Graphite/rolled graphene oxide/carbon nanotube photoelectrode for water splitting of exhaust car solution. Int J Energy Res. 2020;44:7687–97. doi: 10.1002/er.5501.

[32] Rabia M, Aldosari E, Geneidy AHA. Highly flexible poly-O-aminothiophenol/intercalated iodide composite with highly morphological properties for green hydrogen generation from Red Sea Water. Phys Scr. 2024;99:045001. doi: 10.1088/1402-4896/AD2BC5.